Journal of Materials Chemistry A

Accepted Manuscript

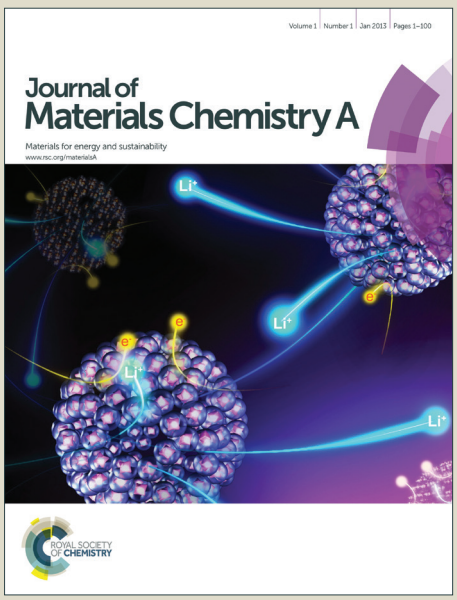

ROYAL SOCIETY OF CHEMISTRY

www.rsc.org/materialsA

Journal Name

RSCPublishing

COMMUNICATION

Scalable Route to $CH_3NH_3PbI_3$ Perovskite Thin Films by Aerosol Assisted Chemical Vapor Deposition

Cite this: DOI: 10.1039/xoxxoooooox

D. S. Bhachu,[a] D. O. Scanlon,[b,c] E. J. Saban,[a] H. Bronstein,[a] I. P. Parkin[a] C. J. Carmalt*[a] and R. G. Palgrave*[a]

Received ooth January 2012,
Accepted ooth January 2012

DOI: 10.1039/xoxxoooooox

www.rsc.org/

Methyl-ammonium lead iodide is the archetypal perovskite solar cell material. Phase pure, compositionally uniform methyl-ammonium lead iodide thin films on large glass substrates were deposited using ambient pressure aerosol assisted chemical vapour deposition. This opens up a route to efficient scale up of hybrid perovskite film growth towards industrial deployment.

The development of hybrid inorganic-organic perovskite (IOP) solar absorbers with remarkable power conversion efficiencies (PCEs) has certainly grabbed the attention of the scientific community.[1,2] Methyl-ammonium lead iodide (MAPI), with PCEs rapidly approaching 20%, has already surpassed the best efficiencies of organic photovoltaics (OPV), dye sensitized solar cells (DSSCs) and the earth abundant inorganic absorbers such as Cu_2ZnSnS_4 (CZTS). The performance of IOPs is now very close to surpassing that of established absorbers such as single crystal GaAs and polycrystaline $Cu(In,Ga)Se_2$.

MAPI crystalizes in the classic ABX_3 perovskite structure, in which Pb^{2+} sits on the corner of the unit cell, octahederally coordinated to six I^-, with the $CH_3NH_3^+$ cations occupying the centre of the cell, and displays a band gap of ~1.5 eV. Originally MAPI was employed as a sensitizer in oxide-based solar cells,[3–5] however, due to its ability to act as an efficient light harvester and charge transporter[6] it has been successfully utilized in high efficiency planar heterojunction-structured solar cells when vapor deposited.[7]

The growth of high-quality thin films of MAPI over a large area is a prerequisite for scale up and practical applications. The most commonly used method for MAPI thin film growth is spin coating,[8–10] where precursors are dissolved in a suitable solvent and film growth occurs on the surface as the solvent is evaporated. An alternative method to achieve greater control of film thickness and reduction of pin-hole defects is to use low-pressure vapour deposition to form a PbI_2 film and to expose the film to a solution of methylammonium in IPA to form MAPI, or alternatively to use dual-source low-pressure vapour deposition.[7,8] Low-pressure vapour deposited films give precise control in film thickness and microstructure but problems arise in controlling the stoichiometry of the inorganic/organic components as PbI_2 often remains in the resulting films and questions arise over the thermal stability of the organic group. A common drawback of each of the aforementioned deposition techniques is that they are difficult or impossible to scale up. There is a limit to the size of substrate that may be spin-coated, and large scale vapour deposition requires a vacuum chamber of prohibitive size.

In this letter we report a simple, one-step, ambient pressure aerosol-assisted chemical vapour deposition (AACVD) process to deposit high quality MAPI thin films on float glass and TiO_2 coated glass substrates. We have deposited phase pure, compositionally uniform MAPI films on substrates 40 cm^2 in area: significantly larger than those previously used for MAPI deposition. Since CVD is highly scalable and is a proven industrial technique, this opens the possibility of efficient scale up of MAPI thin film production. It was recently reported that the bromide analogue of MAPI, $(CH_3NH_3)PbBr_3$ could be synthesized using the AACVD method.[11] Here we show the more active iodide analogue can be similarly deposited using a scalable method, and further demonstrate compositional uniformity, measure the electronic structure and deposit the MAPI film on a flat TiO_2 layer as the first step towards device fabrication using this scalable methodology.

AACVD involves ultrasonic aerosol generation from a precursor solution. The aerosol mist was transported to a cold wall CVD reactor where it was passed over the heated substrate.[12] For MAPI depositions, an equimolar solution of PbI_2 and CH_3NH_3I in N,N-dimethylformamide was used as the precursor solution. Film growth occurred at a substrate temperature of 200°C.[11,13–15] MAPI films were deposited onto float glass substrates, which in some cases had previously been coated with TiO_2 using AACVD from a solution of $Ti(OiPr)_4$ in ethanol. For full experimental details see the Electronic Supplementary Information (ESI).

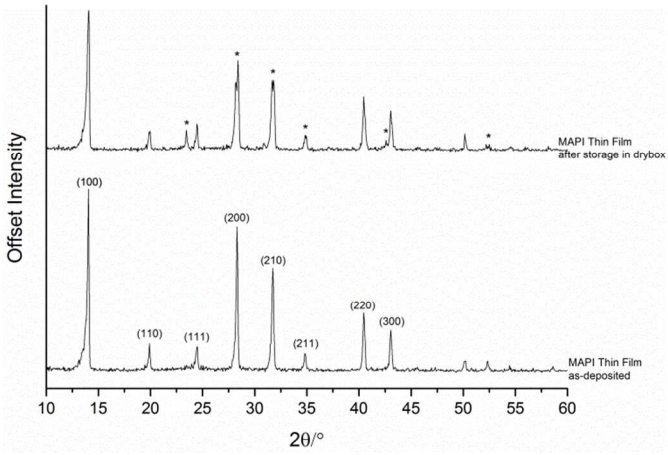

Figure 1 PXRD pattern of $(CH_3NH_3)PbI_3$ film as-deposited (bottom, indexed as cubic) and after storage in a dry box for several days (top), where starred peaks display clear splitting or are otherwise indicative of tetragonal structure.

Figure 1 shows room temperature powder XRD patterns from the as-deposited MAPI film on glass. The XRD pattern taken immediately after deposition and cooling of the sample to room temperature was indexed in the cubic crystal system and the lattice parameter determined as a = 6.2993(4) Å, within the range of values reliably reported for bulk cubic MAPI: 6.276 Å to 6.313 Å.[16,17] The cubic phase of bulk MAPI is stable only above c. 55°C, with a tetragonal form stable at room temperature.[17] Indeed after storage for several days in a drybox, the XRD pattern of the MAPI film showed tetragonal splitting of the diffraction peaks and the appearance of the tetragonal (211) peak around 2θ = 23.5° indicating a phase transition to the tetragonal form had taken place. No PbI_2 or other impurity peaks were observed.

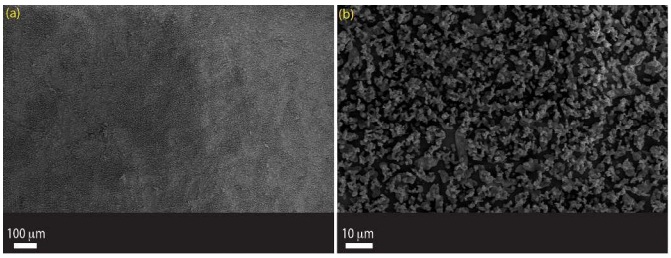

Figure 2 Top down SEM images of as-deposited MAPI thin films by the AACVD reaction of PbI_2 and CH_3NH_3I at 200 °C. (a) A low magnification showing the uniform nature of the films. (b) A higher magnification image showing the rough morphology of the particles.

The film microstructure was inspected using a Field Emission SEM at an accelerating voltage of 5 keV. The secondary electron SEM images of the MAPI thin films are shown in Figure 2. Figure 2(a) shows a low-magnification image of a MAPI thin film and the uniformity of the layer is clearly seen. Figure 2(b) shows a higher magnification image (x 850) of a MAPI thin film and particle sizes can be seen on the nano/micrometer length scale.

XPS was used to determine the stoichiometry and chemical environments present at the surface and also to probe the surface electronic structure of MAPI thin films. Figure 3(a) shows the Pb 4f core level photoemission peak for MAPI thin films; symmetric peak shapes were observed and the binding energy for Pb in CH3NH3PbI3 corresponds to Pb(II), with the $4f_{7/2}$ peak at a binding energy of 137.6 eV.[18–20] Upon extended exposure to the 72 W X-ray beam, the Pb 4f peaks became slightly asymmetric due to the emergence of a minor $4f_{7/2}$ component at 136.5 eV, which we assign as Pb(0).[18] The intensity of this metallic Pb component increased with increasing analysis time, indicating that the sample was slowly decomposing under X-ray irradiation. To mitigate this effect during collection of valence band (VB) spectra, the 400 μm X-ray spot was moved to several positions for shorter analysis times and the resulting spectra summed.

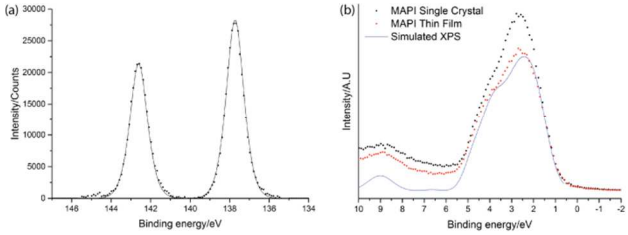

Figure 3 X-ray photoemission spectra of (a) Pb 4f core level of as-deposited MAPI thin film showing the Pb(II) $4f_{7/2}$ and $4f_{5/2}$ transitions with a binding energy of 137.8 eV and 142.7 eV respectively with no metallic Pb component observed and (b) valence band spectrum of as-deposited MAPI thin film, single crystal and simulated XPS VB spectrum obtained from Density Functional Theory (DFT) calculations.

Compositional uniformity was assessed by measuring Pb:I ratios derived from the principle core lines recorded at 72 separate points over a 5.0 x 2.5 cm grid. The mean surface Pb:I ratio was found to be 0.325 with a standard deviation of 0.015, compared with the expected ratio of 0.333. The difference between the mean observed and theoretical Pb:I ratio is 2.5%, which is typical of the error in compositions derived from XPS. Together with the XRD data, this shows that phase pure, compositionally uniform MAPI films have been deposited over large area. Figure 3(b) shows the VB spectra for MAPI thin films and for comparison also with single crystals of MAPI prepared using the method of Kanatzidis et al.[16] The shape of the valence band is almost identical for both sample types. To understand the orbital make-up of the valence band and further confirm the correct material had been deposited, we have compared the XPS spectra to simulated XPS VB spectra calculated using the HSE06 functional[21] with the addition of spin orbit coupling in the VASP code,[22] using the structural model predicted by Walsh et al.[23,24] Further computational details are given in the SI. Simulated XPS VB spectra were obtained by scaling the calculated partial density of states using atomic orbital photoionisation cross-sections[25] and broadening using a 0.47 eV Gaussian function to simulate experimental broadening. Excellent agreement between the experimental and simulated XPS is seen in Figure 3(b), allowing us to identify that the large peak cantered at ~ 3 eV is dominated by I 5p states, with the peak at ~ 9 eV dominated by Pb 6s states.

The absorption spectrum was obtained by treating the optical reflectance of MAPI films on glass with the Kubelka Munk function, $F(R) = \alpha = (1 - R)^2/(2R)$, where R is the reflectivity. The result is shown in figure 4. The optical band gap was determined from the

Kubelka-Munk spectrum by linear extrapolation to the baseline and was found to be 1.54 eV, in good agreement with literature reports.[26,27]

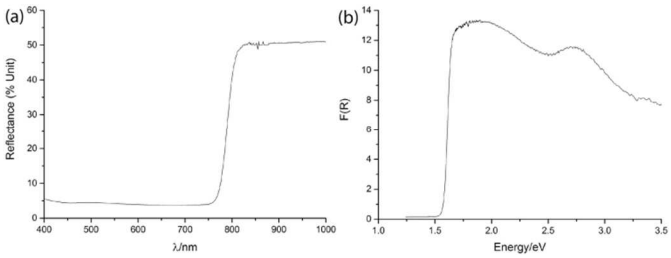

Figure 4 (a) Diffuse reflectance spectra for MAPI thin film and (b) the Kubelka-Munk spectrum for MAPI thin film showing an optical band gap of 1.5 eV.

Conclusions

We report the synthesis and characterization of MAPI thin films deposited on glass substrates from the AACVD reaction of PbI_2 and CH_3NH_3I at 200°C. Films were phase pure, compositionally uniform, displayed the expected optical properties, and the surface electronic structure matched closely with single crystal samples and DFT calculations. This CVD method is carried out at ambient pressure and therefore represents a feasible route to large scale perovskite solar cell production.

We are grateful to the UK EPSRC for funding. RGP acknowledges EPSRC grant EP/K014099/1 and CJC and IPP acknowledge EPSRC grant EP/L017709.

Notes and references

[a] Department of Chemistry, University College London, 20 Gordon Street, London, WC1H 0AJ
[b] University College London, Kathleen Lonsdale Materials Chemistry, 20 Gordon Street, London, WC1H 0AJ, UK
[c] Diamond Light Source Ltd., Diamond House, Harwell Science and Innovation Campus, Didcot, Oxfordshire, OX11 0DE, UK

Electronic Supplementary Information (ESI) available: Full experimental and computational details. See DOI: 10.1039/c000000x/

1. H. J. Snaith, *J. Phys. Chem. Lett*., 2013, **4**, 3623-3630.
2. S. Kazim, M. K. Nazeeruddin, M. GrŠtzel, and S. Ahmad, *Angew. Chem. Int. Ed*., 2014, **53**, 2812-2824.
3. A. K. Chandiran, M. K. Nazeeruddin, and M. Gratzel, *Adv. Funct. Mater*., 2014, **24**, 1615-1623.
4. B. E. Hardin, H. J. Snaith, and M. D. McGehee, *Nat. Photonics*, 2012, **6**, 162-169.
5. M. M. Lee, J. Teuscher, T. Miyasaka, T. N. Murakami, and H. J. Snaith, *Science*, 2012, **338**, 643-647.
6. A. Marchioro, J. Teuscher, D. Friedrich, M. Kunst, R. van de Krol, T. Moehl, M. Gratzel, and J.-E. Moser, *Nat. Photonics*, 2014, **8**, 250-255.
7. M. Liu, M. B. Johnston, and H. J. Snaith, *Nature*, 2013, **501**, 395-398.
8. K. Liang, D. B. Mitzi, and M. T. Prikas, *Chem. Mater*., 1998, **10**, 403-411.
9. A. Kojima, K. Teshima, Y. Shirai, and T. Miyasaka, *J. Am. Chem. Soc*., 2009, **131**, 6050-6051.
10. D. Bi, S.-J. Moon, L. Haggman, G. Boschloo, L. Yang, E. M. J. Johansson, M. K. Nazeeruddin, M. Gratzel, and A. Hagfeldt, *RSC Adv*., 2013, **3**, 18762.
11. D. J. Lewis and P. O'Brien, *Chem. Commun*., 2014, **50**, 6319.
12. P. J. Marchand, I. Hassan, I. Parkin, and C. J. Carmalt, *Dalton Trans*, 2013, -.
13. D. S. Bhachu, S. Sathasivam, G. Sankar, D. O. Scanlon, G. Cibin, C. J. Carmalt, I. P. Parkin, G. W. Watson, S. M. Bawaked, A. Y. Obaid, S. Al-Thabaiti, and S. N. Basahel, *Adv. Funct. Mater*., 2014,
14. R. G. Palgrave and I. P. Parkin, *J. Am. Chem. Soc.*, 2006, **128**, 1587-1597.
15. D. S. Bhachu, G. Sankar, and I. P. Parkin, *Chem. Mater*., 2012, **24**, 4704-4710.
16. C. C. Stoumpos, C. D. Malliakas, and M. G. Kanatzidis, *Inorg. Chem*., 2013, **52**, 9019-9038.
17. T. Baikie, Y. Fang, J. M. Kadro, M. Schreyer, F. Wei, S. G. Mhaisalkar, M. Graetzel, and T. J. White, *J. Mater. Chem*. A, 2013, **1**, 5628.
18. R. Lindblad, D. Bi, B. Park, J. Oscarsson, M. Gorgoi, H. Siegbahn, M. Odelius, E. M. J. Johansson, and H. Rensmo, *J. Phys. Chem. Lett*., 2014, **5**, 648-653.
19. D. S. Bhachu, S. Sathasivam, C. J. Carmalt, and I. P. Parkin, *Langmuir*, 2014, **30**, 624-630.
20. D. J. Payne, R. G. Egdell, D. S. L. Law, P.-A. Glans, T. Learmonth, K. E. Smith, J. Guo, A. Walsh, and G. W. Watson, *J. Mater. Chem*., 2007, **17**, 267.
21. A. V. Krukau, O. A. Vydrov, A. F. Izmaylov, and G. E. Scuseria, *J. Chem. Phys*., 2006, **125**, 224106.
22. G. Kresse, *Phys. Rev. B*, 1999, **59**, 1758-1775.
23. F. Brivio, A. B. Walker, and A. Walsh, *APL Mater*., 2013, **1**, 042111.
24. F. Brivio, K. T. Butler, A. Walsh, and M. van Schilfgaarde, *Phys. Rev. B*, 2014, **89**.
25. J. J. Yeh and I. Lindau, *At. Data Nucl. Data Tables*, 1985, **32**, 1-155.
26. H.-S. Kim, J.-W. Lee, N. Yantara, P. P. Boix, S. A. Kulkarni, S. Mhaisalkar, M. GrŠtzel, and N.-G. Park, *Nano Lett*., 2013, **13**, 2412-2417.
27. H.-S. Kim, C.-R. Lee, J.-H. Im, K.-B. Lee, T. Moehl, A. Marchioro, S.-J. Moon, R. Humphry-Baker, J.-H. Yum, J. E. Moser, M. Gratzel, and N.-G. Park, *Sci. Rep.*, 2012, **2**.